A Direct Approach to Progressive Buckling Design Considering Ratcheting Deformation

Fang Liu[1], Jian-Guo Gong[1], Hao feng Chen[1,2]*, Fu-Zhen Xuan[1]*

[1] Key Laboratory of Pressure Systems and Safety, School of Mechanical and Power Engineering, East China University of Science and Technology, Shanghai, 200237, China

[2] Department of Mechanical & Aerospace Engineering, University of Strathclyde, Glasgow, G1 1XJ, UK

*Email: haofeng.chen@strath.ac.uk; fzxuan@ecust.edu.cn

Abstract

In this paper, the Bree diagram is extended to consider the progressive buckling failure and a direct approach for structural progressive buckling design considering ratcheting deformation is developed. Firstly, the progressive buckling mechanism of structures subjected to the combination of constant and cyclic loadings is sufficiently discussed. Then, a two-stage direct approach is developed based on the Linear Matching Method and nonlinear buckling analysis, which can generate progressive buckling design curves in the extended Bree diagram. To illustrate the application of the direct approach to progressive buckling design, a cylindrical shell model with an opening is provided as a numerical example. Furthermore, geometrical effects, e.g. the opening size and the shell thickness, on the progressive buckling limit are investigated. Formulas for progressive buckling design of cylindrical shells with various geometrical parameters are derived by fitting curves. Compared with other methods, the direct approach could predict accurate progressive buckling load.

Keywords

Bree diagram; Direct approach; Progressive buckling; Ratcheting deformation; Linear Matching Method

1. Introduction

Buckling is a critical failure mode for structures subjected to compressive stress [1-3] such as cylindrical shells [4,5] and spherical shells [6,7] subjected to external pressure, cylindrical shells [8-10] under axial compression and torispherical as well as ellipsoidal heads under internal pressure[11-13]. During the service time, the structures will also inevitably experience cyclic loading, such as thermal loading [14，15] and seismically induced cyclic loading [16,17]. For the structures subjected to a constant compressive loading which is smaller than the critical buckling load and to a cyclic secondary stress due to cyclic loading, it is expected that for certain combination of these loadings, the deformation increases sharply after a given number of cycles and buckling failure takes place. In such a case, buckling occurs due to the progressive increasing of the ratcheting deformation under the effect of the cyclic secondary stress. That is called progressive buckling [18].

In general, the failure mechanism of structures subjected to combinations of constant loading and cyclic loading is known as either a local low cycle fatigue failure (alternating plasticity) or ratcheting with excessive deformation (incremental plasticity) and many works have been reported on both failure modes [19-24]. For the structures subjected to compressive loading, the additional displacement and residual stress due to the progressive plastic strain lead to buckling failure of these structures. Thus the progressive buckling is another detrimental failure mode in engineering components. As known to all, the range of structural responses subjected to cyclic loading is usually illustrated through the Bree diagram [25,26], which indicates that the combination of loadings leads to various cyclic material and structural behaviors. In previous studies, a number of direct methods have been proposed which can compute the shakedown boundary and ratcheting boundary quickly by making a few hypotheses [27-34]. As one of the direct approaches that modifies the elastic modulus, the Linear Matching Method (LMM) [30-34] could be used to predict shakedown and ratcheting limits in Bree problem directly. However, the limit of progressive buckling design is not included in the Bree diagram until now. Therefore, to ensure the integrity of components under the

action of constant and cyclic loadings, much effort should be paid to the progressive buckling design.

In previous studies, some experimental and theoretical works about the progressive buckling have been reported. Brouard et al. [35] observed the phenomenon of destabilization in the case of cyclic test of cylindrical tube under constant axial compression and cyclic torsional deformation, which is firstly evidenced by experiment that the critical buckling load is decreased due to the cyclic deformation. Quoc et al. [36] theoretically studied the progressive buckling behavior of an axially compressed beam subjected to thermal cyclic loading, and an estimated critical loading has been found to guard against progressive buckling failure. Devos, Gontier and Hoffmann [37] studied the case of a beam subjected to constant compressive loading and cyclic thermal stress, taking initial geometrical imperfections into account. They modeled the behavior of elastic-plastic hinges by using minimum monotonic tensile curves, and a limit of buckling design has been defined with this model. Because the actual cyclic behavior of the material is not considered and the structures as well as loading conditions are different for other cases, the Gontier's limit is rather conservative compared with the experimental results for cylindrical shell. Then Clement et al. [18] proposed a practical design rule based on the Gontier's method to prevent progressive buckling failure of cylindrical shell under axial load and cyclic twist deformation. It is found a better agreement of shape between the design diagram and the lower boundary of buckling experimental results, than between this latter and the Gontier's curve. This method, however, is limited to these structures with small initial geometrical imperfections. In fact, buckling failure, usually caused by large displacement, is very sensitive to initial geometrical imperfections [38-41]. So the Clement's method could not predict the progressive buckling load for structures with large initial geometrical defects. Besides, the cycle number, which is an important factor in progressive buckling failure according to experimental results [18], is not considered in the Clement's method. As mentioned above, methods for progressive buckling design are based on some hypotheses, such as simplified material model, small initial geometrical imperfections, which predict inaccurate results. Meanwhile, these methods are limited to simple structures and there

is no unified method for the design of complicated engineering components. Therefore, more efforts are required for the research of progressive buckling design.

Recently, numerical analysis is applied to investigate the buckling behavior of structures subjected to constant compressive stress [42-46]. In these works, the nonlinear buckling analysis, e.g. the arc-length algorithm, is most often used to predict the buckling load. Besides, the buckling behavior under cyclic loading is also investigated by numerical analysis [47-51]. For example, Jimbo et al. [47] and Koo et al. [48] studied the thin-walled cylindrical shell which is prone to buckling subjected to a cyclic moving axial temperature gradient. It is found that thermal buckling occurs at the free edge region when the ratcheting strain accumulates in the moving zone. Dicleli and Mehta [49] simulated the buckling behavior of steel braces under cyclic axial force-deformation. Hassan et al. [50] analyzed the buckling behavior of square and rectangular structural steel hollow section under cyclic axial loading using the commercial finite element package ABAQUS [52]. Three modes of geometrical imperfections are considered in analyses and a good agreement is found between numerical and experimental results. In the design code RCC-MRx [53], the effect of cyclic secondary stress on buckling load is considered and two methods are proposed based on elastic analysis. In both methods, effective stress determined on the basis of primary stress and secondary stress should be limited to the allowable stress. However, the results predicted by RCC-MRx are conservative for cases less sensitive to geometrical imperfections, such as the buckling of cylindrical shell under bending or shear [54]. As mentioned above, although the finite element method has been applied to buckling analysis, most of methods are only used to the condition that constant loading or cyclic loading occurs separately. There is no unified numerical method that could predict progressive buckling limit accurately.

To guard against progressive buckling failure of structures subjected to the combination of constant and cyclic loadings, the Bree diagram is extended to consider the progressive buckling failure. A direct approach based on the LMM and nonlinear buckling analysis is proposed to predict the limit of progressive buckling in the Bree diagram. The structure of this work is arranged as follows: firstly, the mechanism of

progressive buckling is discussed comprehensively in section 2 and numerical procedures for progressive buckling design developed by the authors are described in section 3. Then, numerical models are provided in section 4. Results and discussions are reported in section 5, including effects of dimension and material property on buckling and progressive buckling failure. In addition, formulas for progressive buckling design of cylindrical shells are derived by fitting curves. Finally, conclusions drawn through this investigation are summarized in section 6.

2. Progressive buckling mechanism

For general phenomena of structure under cyclic loading condition, e.g. shakedown and ratcheting, the Bree diagram could be used to illustrate the structural response. As mentioned above, for structures subjected to compressive loading, if ratcheting deformation is observed, the additional displacement and residual stress due to the progressive plastic strain lead to progressive buckling failure, which is another crucial design limit in engineering practice. In this section, the general cyclic problem and the mechanism of progressive buckling are discussed in detail.

2.1. General cyclic problem

In general, the range of all possible structural responses subjected to combined constant loading and cyclic loading is most often illustrated through the Bree diagram. The Bree diagram has been developed for different structures subjected to different combinations of loadings [55-58] and it is also the foundation of ratcheting assessment in ASME III NH [59]. A schematic illustrating the Bree diagram is shown in Fig. 1 [60]. The abscissa is the ratio of mechanical loading P (primary stress) to limit loading P_L and the ordinate is the ratio of thermal loading ΔT (secondary stress) to the loading ΔT_0, where ΔT_0 is the temperature range required for yield initiation in the absence of the mechanical loading. As shown in Fig. 1, if $P/P_L + \Delta T/\Delta T_0<1$, elastic response takes place in the whole structure. In the domain of $P/P_L>1$, plastic collapse occurs on the first loading cycle. In the shakedown regime, local plastic strain occurs in the first several cycles, giving rise to residual stress that prevents plastic deformation and results

in a purely elastic behavior in subsequent cycles. Alternating plasticity results from loading beyond the shakedown limit. Here the increment of plastic strain obtained during the first half of each loading cycle is followed by a plastic strain increment of equal magnitude but opposite sign during the second half. No net strain accumulates during each cycle but the structure ultimately fails by fatigue. Ratcheting refers to the condition in which a net increment of plastic strain accumulates during each cycle, eventually resulting in rupture. For thin-walled structures, buckling is another failure mode in addition to fatigue and ratcheting. If the combined loads are in the ratcheting region, the plastic strain increases with the increasing of load cycle, and this would reduce the buckling load carrying capacity, and progressive buckling will then occur. The local fatigue crack initiation and propagation may not significantly contribute to the progressive buckling.

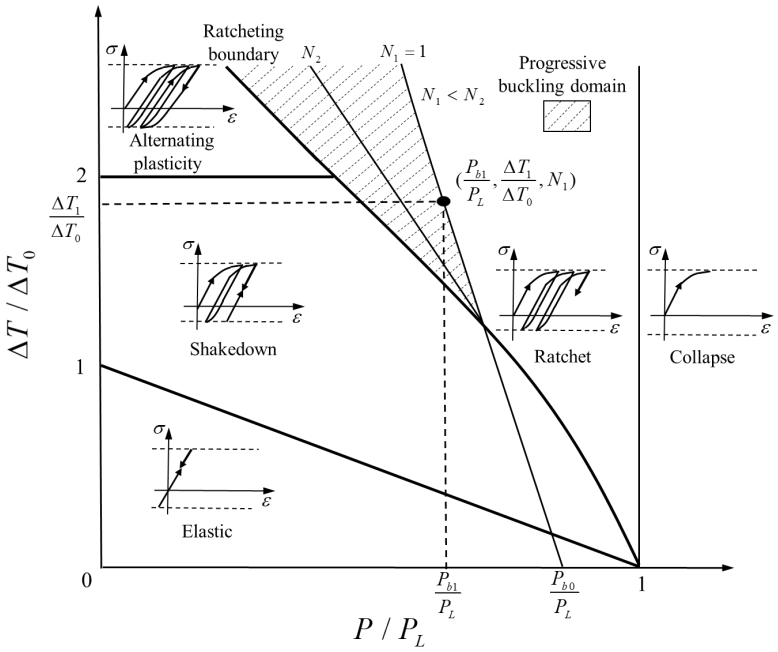

Fig. 1. Bree diagram considering progressive buckling failure, including elastic, shakedown, alternating plasticity, ratcheting and progressive buckling domains. The shadow region represents the progressive buckling domain, where N_1 and N_2 denote number of cycles. P_{b0} is the buckling load in the absence of the thermal loading and P_{b1} is the progressive buckling load corresponding to the number of cycle N_1 and the range of thermal loading ΔT_1.

To get the shakedown and ratcheting boundaries in the Bree diagram, the LMM,

considering elastic-perfectly-plastic material and small deformation, is developed to predict shakedown and ratcheting limits directly. The limit load P_L, i.e. the load carrying capacity, is also determined as a special case of shakedown analysis. However, the limit of progressive buckling is not included in the Bree diagram until now. For structures prone to buckle, the buckling load, usually smaller than the limit load, is the critical load for these structures. Therefore, it will predict risky design limit if the buckling failure is not taken into account.

2.2. Progressive buckling behavior

For some structures subjected to compressive stress, buckling instead of plastic collapse is the governing failure mode [61]. Based on elastic buckling theory, the buckling pressure of cylindrical shell under axial load could be expressed as Eq.(1) [1], where P_{b0} denotes buckling pressure, ε_{cr} is the critical strain when buckling takes place, E is Young's modulus, t is thickness, R is radius, and v is Passion ratio. If the mechanical properties of the material beyond the yield stress, the tangent modulus E_t instead of E is introduced in the Eq. (1) to predict the buckling pressure. In design code RCC-MRx [53], the critical strain, which could be predicted by thickness t, radius R and Passion ratio v, is used to predict the allowable buckling pressure. According to the buckling theory, the strain is an important parameter in buckling design. As shown in Eq. (2), the total strain consists of elastic strain and plastic strain. It could be deduced that the ratcheting strain will have effect on buckling pressure.

$$P_{b0} = E\varepsilon_{cr} = E\frac{t}{R\sqrt{3\,(1-\nu^2)}} \tag{1}$$

$$\varepsilon_{total} = \varepsilon_e + \varepsilon_p \tag{2}$$

The theoretical solution as Eq. (1) could only be used to buckling design of simple case. The effect of ratcheting strain on buckling load is a complicated buckling problem and the nonlinear buckling analysis (Riks analysis) could be used for this complex buckling analysis. In Riks analysis, the applied load is governed by a load proportional factor λ. The applied load P is defined as Eq. (3), where P_1 is the load in Riks step and P_0 is the dead load in previous steps.

$$P = P_0 + \lambda P_1 \tag{3}$$

For progressive buckling, the issue is actually to investigate the effect of cyclic loading (secondary stress) on the buckling load (primary stress). In fact, both primary and secondary stress could result in buckling failure individually. For buckling caused by primary stress, e.g. buckling of a cylindrical shell under uniform axial loading, it is a type of buckling caused by force-controlled loading. For buckling caused by secondary stress, e.g. buckling of plate subjected to thermal stress, it results from deformation-controlled loading. The characteristic of force-controlled loading is that they cannot disappear when plastic deformation occurs, while deformation-controlled loading can disappear by this way. For most components in engineering, buckling failure usually takes place because of the force-controlled loading. For the deformation-controlled buckling, it is characterized by the immediate reduction of strain induced load on the initiation of buckling, and by the self-limiting nature. Even though it is self-limiting, deformation-controlled loading must be considered to guard against failure by excessive strain, and interaction with force-controlled loading [48,59]. For progressive buckling failure, the prediction of design limit is much complicated because the force-controlled loading (primary stress) and deformation-controlled loading (secondary stress) occur simultaneously. On the one hand, the plastic strain accumulates at each cycle. This progressive deformation leads to buckling failure at a lower buckling load than expected. On the other hand, the cyclic secondary stress is added to primary stress, which increases the risk of buckling.

To predict the progressive buckling design limit, the Bree diagram is extended to progressive buckling design. Figure 1 schematically illustrates the Bree diagram considering progressive buckling failure, and the progressive buckling domain is located in the ratcheting region, where N_1 and N_2 denote the number of cycles and the value of N_2 is greater than N_1. P_{b0} is the buckling load in the absence of the thermal loading and P_{b1} denotes the progressive buckling load corresponding to the number of cycle N_1 and the range of thermal loading ΔT_1. It could be found that the progressive buckling load is decreased with the increasing of thermal loading. Whereas, the plasticity due to cyclic secondary stress has no noticeable effect on the limit load P_L. Besides, with the increasing of cycles, such as the number of cycles increasing from N_1

to N_2, the buckling load is decreased due to the increased accumulated deformation. It is also seen that the progressive buckling load is affected by the cyclic thermal loading in shakedown region. This is because the plastic deformation takes place in the first cycle, which could decrease the progressive buckling load.

It is concluded that the cycle number as well as the secondary stress have effects on the value of progressive buckling load. To obtain a design limit of progressive buckling in the Bree diagram, it is firstly necessary to determine the traditional Bree diagram. Under certain combination of primary and secondary stresses, the progressive buckling load corresponding to a determined cycles could be predicted by nonlinear buckling analysis. Finally, the design point, such as (P_{b1}/P_L, $\Delta T_1/\Delta T_0$, N_1) in Fig. 1, could be predicted. Based on above procedures, the progressive buckling design curves in the Bree diagram could be obtained.

3. A direct approach to progressive buckling design

In this section, a direct approach to the progressive buckling design is proposed based on the extended Bree diagram. The whole numerical procedure has been plotted in the form of a flowchart, as shown in Fig. 2. There are two stages in the direct approach as depicted.

In the first stage, the main objective is to determine the traditional Bree diagram by the LMM. In the process, the extreme loading history of structure should be firstly determined. According to the loading history as well as the structural geometry, it could be concluded that whether the structure is prone to buckling. For example, thin-walled structures under compressive loading usually suffer from buckling failure. If the structures have no risk of buckling, the progressive buckling is excluded. Otherwise, the LMM is implemented to get the Bree diagram of the structures.

In the second stage, the progressive buckling limit in the Bree diagram will be obtained. Firstly, nonlinear buckling analysis, such as Riks analysis in ABAQUS, is applied to get the buckling load P_{b0} in the absence of cyclic secondary stress. Then ratcheting analysis is conducted via step by step analysis with certain combination of

constant and cyclic loadings, and the constant loading applied should be decreased from P_{b0}. The most risky state for buckling during the ratcheting analysis should be obtained. In general, the most risky state is that when the maximum compressive secondary stress is added to the primary stress or the deformation reaches its maximum value. Then progressive buckling load P_b of the critical state could be predicted by nonlinear buckling analysis. Comparing the value of P_b with the constant primary load applied in ratcheting analysis, if the value of P_b is equal to the constant load in ratcheting analysis, a progressive buckling design point is obtained. If not, reset the constant load in the ratcheting analysis and repeat the above procedures until the progressive buckling load P_b is equal to the constant load. Finally, the progressive buckling limit in Bree diagram, such as the design limit in Fig. 1, could be obtained via the proposed direct approach.

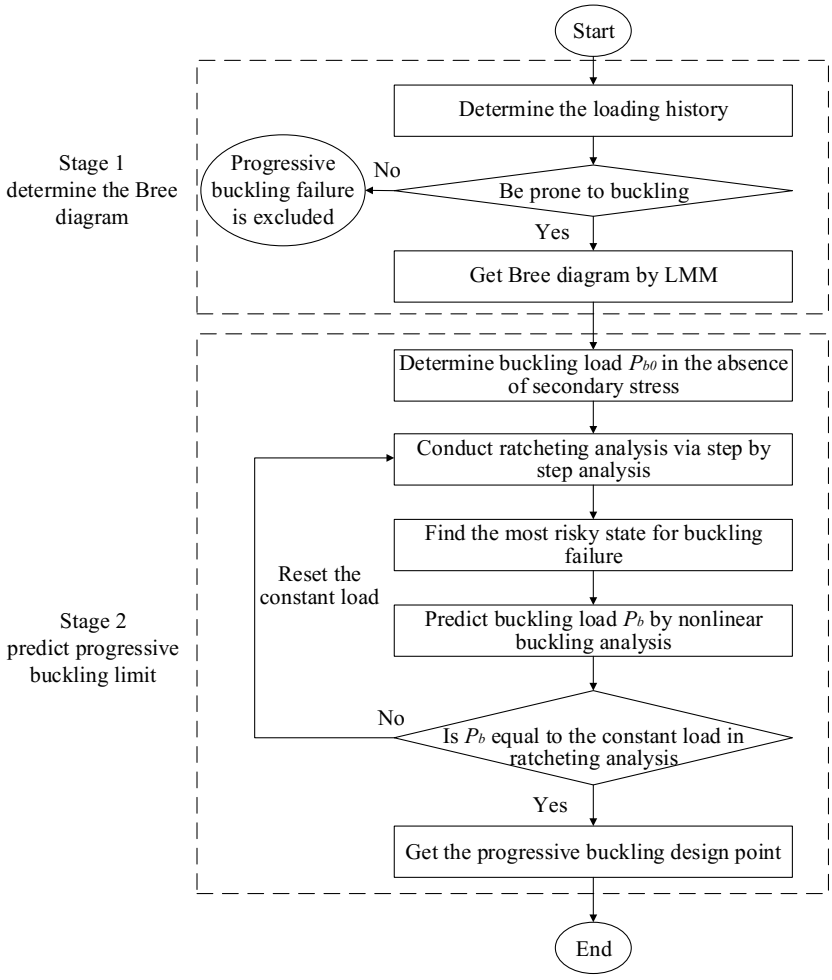

Fig. 2. Flowchart of the direct approach to progressive buckling design, including two stages. In the first stage, the traditional Bree diagram is determined by the LMM. In the second stage, the progressive buckling limit in the Bree diagram will be obtained via

step by step analysis and nonlinear buckling analysis.

4. Numerical model

In this section, numerical example is provided to illustrate the application of the direct approach to progressive buckling design. Thin-walled cylindrical shell subjected to uniform axial pressure and cyclic thermal loading is taken as an example because of its wide use in engineering applications.

4.1. Geometrical and mesh model

Due to the functional requirement or unexpected condition, such as corrosion, opening is usually included in the cylindrical shell, and buckling is one of the main failure modes for the cylindrical shell with an opening. So the model adopted for numerical analysis is a cylindrical shell with an opening at the middle height of the shell. The length of the cylindrical shell L is 6000mm and the inner radius R_i is 1000mm. Various shell thicknesses t, semi-major axes a and semi-minor axes b of opening are chosen to investigate the effects of geometrical parameters on the progressive buckling load and the detailed parameters are shown in Table 1.

Table 1 Geometrical parameters of cylindrical shells

Length of cylindrical shell L/mm	Inner radius of cylindrical shell R_i/mm	Shell thickness t/mm	Semi-major axis of opening a/mm	Semi-minor axis of opening b/mm
6000	1000	5~30	200~800	200~800

As shown in Fig. 3, a three dimensional finite element model using ABAQUS is established to perform the progressive buckling analysis. The structure is discretized by the 20-node quadratic brick element with a reduced integration scheme (C3D20R). In order to capture the buckling mode of the cylindrical shell accurately, the structure around the opening is meshed using a higher finite element density than that in other regions. It should be stated that the element number depends on the model geometry. Taking the model with a=200mm, b=200mm and t=12mm as an example, 19,904 elements and 110,611 nodes are generated after mesh generation. Two layers of

elements are considered through the thickness, which could give accurate results because the thickness in analysis is small and the distribution of stress is almost linearly varying through the thickness under the combined load. It has been proved that the effect of element number on analysis results is insignificant with such amount of element.

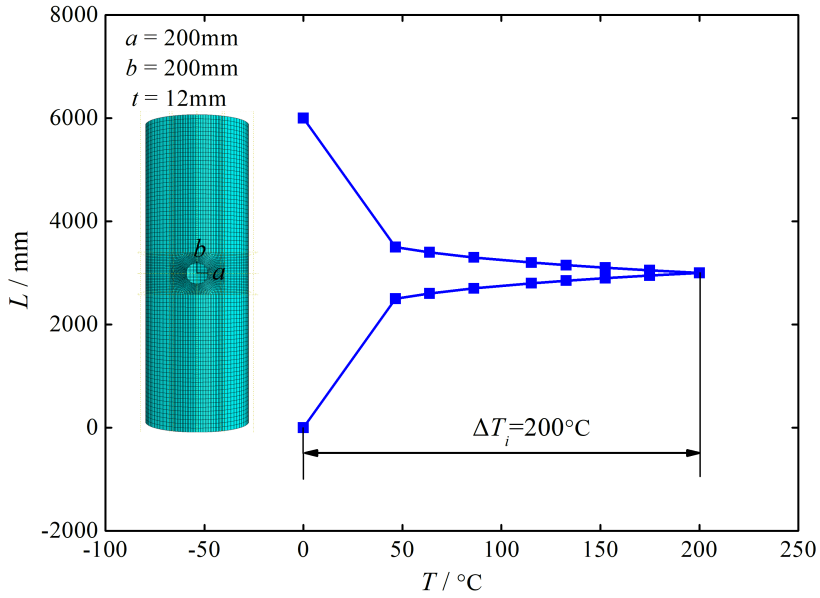

Fig. 3. Mesh model with a=200mm, b=200mm and t=12mm, where a, b and t are the semi-major axis of opening, the semi-minor axis of opening and shell thickness, respectively. Temperature distribution of the cylindrical shell, shown as the solid blue line with rectangle. The applied highest reference range of temperature ΔT_i is 200°C.

4.2. Material properties

The material model used is assumed to follow the elastic-perfectly-plastic behavior. For usually used material in elevated temperature, the yield stress of 2.25Cr-1Mo-V is about 300MPa-400MPa and the yield stress of 316SS is about 100MPa-200MPa. To investigate the material effect on the buckling failure, the yield stresses ranging from 100MPa to 400MPa are used in analyses. Besides, the Young's modulus, Poisson's ratio and thermal expansion coefficient are 220GPa, 0.3 and 2.2e-5, respectively. The material properties used for analysis are presented in Table 2.

Table 2 Material properties

Young's modulus /GPa	Yield stress /MPa	Poisson's ratio	Thermal expansion coefficient
220	100~400	0.3	2.2e-5

4.3. Loads and boundary conditions

As shown in Fig.4, a constant axial pressure is applied to the top end face of the structure and a cyclic thermal loading is applied to the shell. The distribution of temperature is shown in Fig. 3 and it is symmetrical about the middle height of the cylindrical shell. The highest temperature is located at the middle of the structure and the temperature decreases along the vertical (Z direction) direction. The applied highest reference range of temperature ΔT_i in Fig. 3 is 200℃. Compressive secondary stress and large ratcheting strain could take place around the opening under the distribution of temperature shown in Fig. 3, which could make it easier to investigate the effect of ratcheting strain on buckling failure.

For the boundary conditions, it could be seen in Fig. 4 that the vertical (Z direction) displacement of the bottom end face is eliminated and the displacements at point O in X and Y direction are fixed as zero. Furthermore, plain conditions are imposed on the top end face of the model.

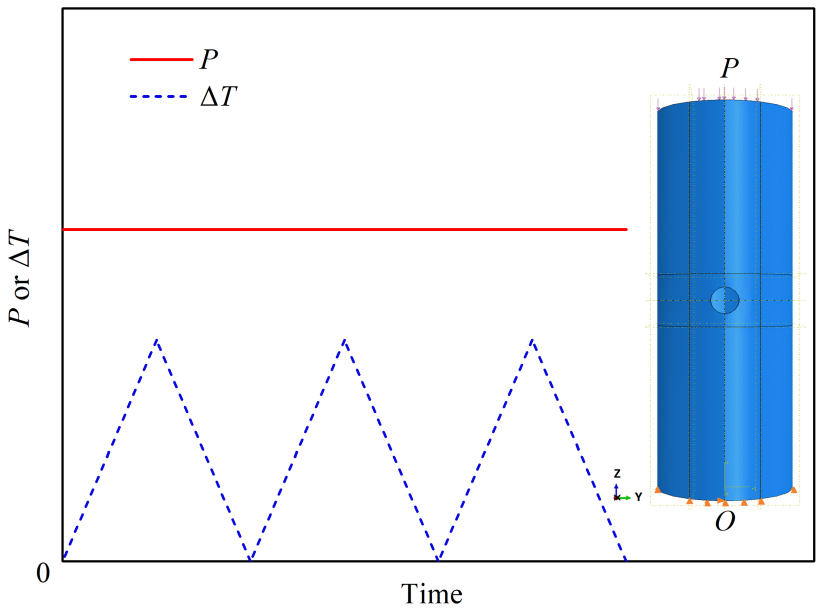

Fig. 4. Loading history and boundary condition of the cylindrical shell. The solid red line and the dashed blue line represent the pressure and the cyclic thermal load, respectively. The vertical (Z direction) displacement of the bottom end face is eliminated and the displacements at point O in X and Y direction are fixed as zero.

4.4. Progressive buckling analysis

4.4.1. The direct approach

Based on the direct approach described in section 3, firstly, the LMM is applied to get the shakedown and ratcheting boundaries in the traditional Bree diagram. Then Riks analysis is applied to predict the progressive buckling limit of cylindrical shell considering ratcheting deformation. To calculate the ratcheting deformation, step by step analysis, considering material nonlinearity, is conducted with certain cycles. It is noted that the most risky state for buckling is on the loading of last cycle when thermal loading is applied to the cylindrical shell and ratcheting deformation reaches its maximum value.

4.4.2. The Clement's method

Clement et al. [18] proposed a method that can define a minimum limit of instability regardless of number of cycles. Design curves provided by Clement for different values of the stiffness parameter ξ are shown in Fig. 5. The stiffness parameter ξ is defined as Eq. (4), where P_E is the critical Euler pressure which could be predicted by elastic buckling analysis and P_L is the limit pressure. For different values of initial geometrical

imperfection δ, shown as Eq. (5), the design curves are different. For δ=0, the design curves are shown as Fig. 5, where the abscissa is the ratio of secondary stress ΔQ to mechanical loading P (primary stress) and the ordinate is the ratio of mechanical loading P (primary stress) to the buckling load in the absence of cyclic secondary stress P_{b0}. Until now, the method could only be used to the cases with δ<0.1. Besides, the cycle number is not considered in the Clement's method, so it would predict conservative result for structure with small cycle number.

$$\xi = P_E / P_L \tag{4}$$

$$\delta = d / t \tag{5}$$

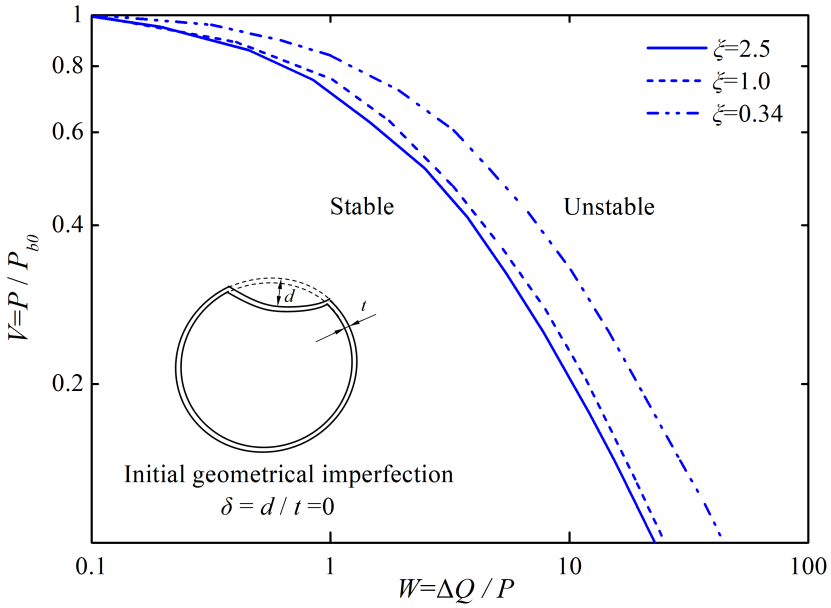

Fig. 5. Clement's design curves for progressive buckling. The initial geometrical imperfection δ=0. The factor d represents the maximum initial displacement and t is the thickness. The solid line, the dashed line and the dashed-dotted-dotted line represent design curves with stiffness parameter ξ of 2.5, 1.0 and 0.34, respectively.

5. Results and discussions

5.1. Effects of geometry and material property on buckling failure

As mentioned in section 2, buckling and plastic collapse are two significant failure modes. In this section, the effects of geometrical parameter and material property on the buckling failure and plastic collapse are investigated.

5.1.1. Effect of ratio of thickness to inner radius

It is known that the buckling is a phenomenon related to structural dimension [62,63]. To have a general understanding of the buckling behaviors of the cylindrical shells with opening, their buckling behaviors are firstly investigated with various ratios of inner radius R_i to thickness t. As shown in Fig. 3, the circle opening with a=200mm and b=200mm is located at the middle height of the cylindrical shell. The inner radius of cylindrical shell R_i is constant as 1000mm, and thicknesses t ranging from 5mm to 30mm are considered in finite element analysis. The Young's modulus and Poisson's ratio used for analysis are presented in Table 2, and the yield stress is fixed as 300MPa.

The failure modes at point C_1 and C_2 of cylindrical shells predicted by Riks analysis with two ratios R_i/t of 83.3 and 45.4 are displayed in Fig. 6. For both ratios, wrinkles take place around the left and right boundary of the opening. The maximum displacement with ratio R_i/t of 45.5 is smaller than that with ratio R_i/t of 83.3. For the pressure-displacement curves shown in Fig. 6, the pressure increases with the displacement at the start of the analysis. Then the critical status, shown as C_1 in Fig. 6, is reached and the shell falls into the post-buckling stage. During this stage, the unloading process takes place where the softening of the structure occurs and the negative stiffness appears, and the displacement decreases. At this time, the structure must release strain energy to remain in equilibrium.

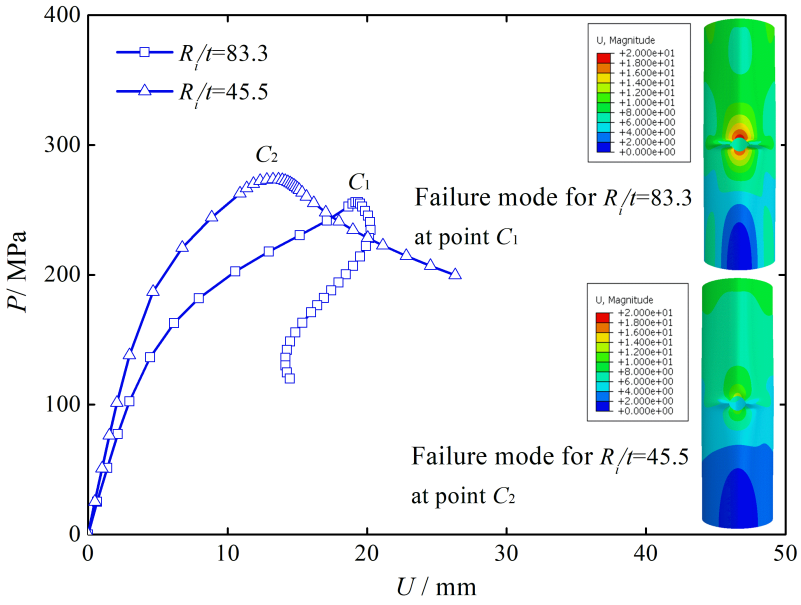

Fig. 6. Pressure-displacement curves and failure modes for models with R_i/t=83.3 and R_i/t=45.5 in Riks analysis. The curves for R_i/t=83.3 and R_i/t=45.5 are shown in the line

with rectangle and the line with triangle, respectively. The upper contour is the failure mode with R_i/t=83.3 and the lower is the failure mode with R_i/t=45.5. The yield stress σ_y is 300MPa and deformation scale factor of contour is 10.

The critical pressures with various geometries and the plastic strain distributions of models with R_i/t=83.3 and R_i/t=45.5 at critical state are displayed in Fig. 7. The grey zone represents the elastic region and the others are plastic regions. It is seen that the difference between plastic buckling and plastic collapse is that the plastic strain mainly takes place around the boundary of the opening as well as the upper and lower boundaries of the shell on initiation of buckling, while the plastic strain occurs through the axial direction of the shell for plastic collapse. Besides, it is shown in Fig. 7 that the effect of ratio R_i/t on limit pressure is insignificant and the limit pressure is smaller than the yield stress due to the opening. While for buckling pressure, it is decreased with the increasing ratio R_i/t, which is due to the decreasing of stiffness caused by small value of t. From the results shown in Fig. 7, it is concluded that the failure modes change from plastic collapse to buckling with the increasing of ratio R_i/t. This is because large displacement takes place in the thin-walled shell and results in buckling failure, while for thick shell, the stiffness is large enough to guard against large displacement and the plastic collapse instead of buckling becomes the governing failure mode.

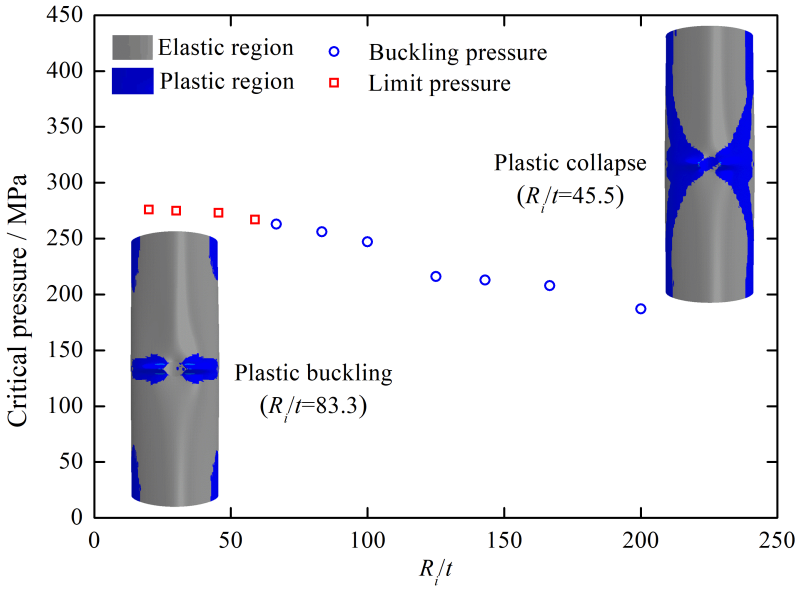

Fig. 7. Critical pressures and plastic strain distributions for various ratios of thickness to inner radius. The blue circle is the plastic buckling pressure and the red rectangle is

the limit pressure for plastic collapse. The left upper contour and the right lower contour are the distributions of plastic strain on the start of plastic buckling and plastic collapse. The yield stress σ_y is 300MPa and deformation scale factor of contour is 10.

5.1.2. Effect of yield stress

For plastic collapse, the limit load is proportional to the yield stress. However, there is no idea about the effect of yield stress on buckling failure of the cylindrical shell with opening. In this section, the effect of yield stress on buckling pressure of cylindrical shell is investigated. The semi-major axis a and semi-minor axis b of opening are 200mm. The inner radius R_i and thickness t of cylindrical shell are 1000mm and 12mm, respectively. The Young's modulus and Poisson's ratio used for analysis are presented in Table 2. The yield stresses ranging from 100MPa to 400MPa are considered in analyses.

The failure modes at point C_3 and C_4 of cylindrical shells predicted by Riks analysis with two yield stresses of 300MPa and 100MPa are displayed in Fig. 8. The failure modes are quite similar but the maximum displacement with yield stress of 100MPa is smaller than that with yield stress of 300MPa. For critical pressure, i.e. the maximum pressure in the pressure-displacement curve, the value with yield stress of 100MPa is smaller than that with yield stress of 300MPa.

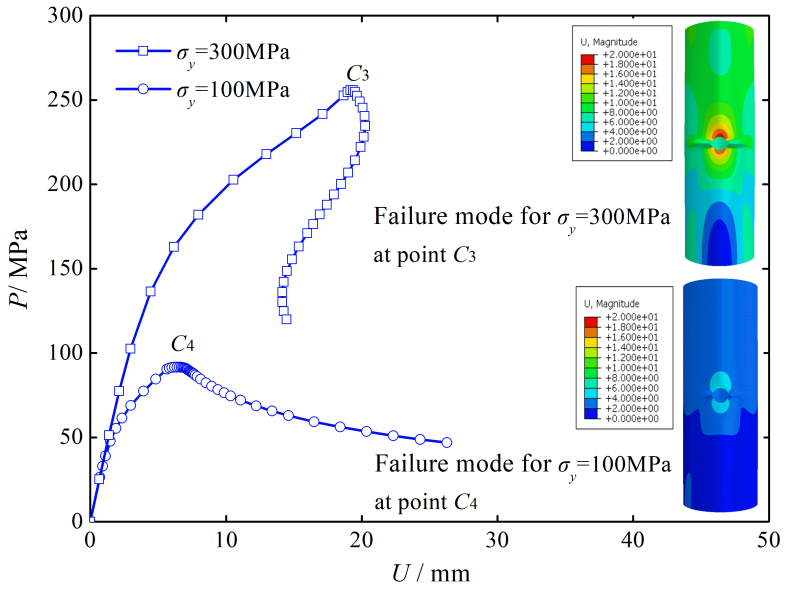

Fig. 8. Pressure-displacement curves and failure modes for models with yiled stress σ_y=300MPa and σ_y =100MPa in Riks analysis. The curves for σ_y=300MPa and σ_y

=100MPa are shown in the line with rectangle and the line with circle, respectively. The upper contour is the failure mode with σ_y=300MPa and the lower is the failure mode with σ_y=100MPa. The ratio R_i/t is fixed as 83.3 and `deformation scale factor of contour is 10`.

The critical pressures and plastic strains predicted by Riks analysis with various yield stresses are shown in Fig. 9. From the distributions of plastic strain, it can be concluded that plastic collapse is the governing failure mode for the model with yield stress of 100MPa, while the plastic buckling takes place when the yield stress is equal to 300MPa. For limit pressure, it is proportional to the yield stress as the dashed red line shown in Fig. 9, while the buckling pressure exhibits a nonlinear growth with the increasing of yield stress. It is also seen that the failure modes change from plastic collapse to plastic buckling with the increasing of yield stress. The reason for the change of failure mode is that both limit pressure and buckling pressure increase with the yield stress, but the limit pressure presents a more significant increment than the buckling pressure. Therefore, the plastic buckling instead of plastic collapse becomes the governing failure mode for cases with larger yield stress.

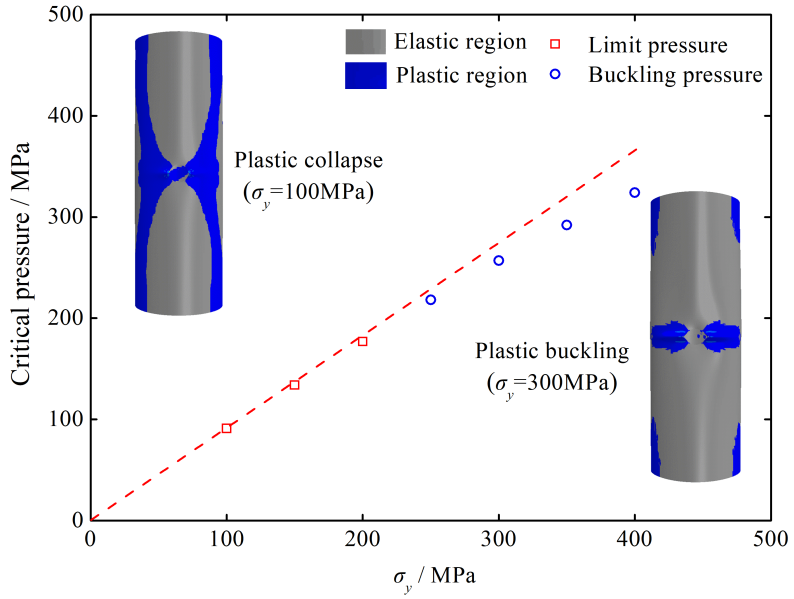

Fig. 9. Critical pressures and plastic strain distributions for various yield stresses. The blue circle is the plastic buckling pressure and the red rectangle is the limit pressure for plastic collapse. The dashed red line shows that limit pressure is proportional to yield stress. The left upper contour and the right lower contour are the distribution of plastic

strain on the start of plastic collapse and plastic buckling, respectively. The ratio R_i/t is fixed as 83.3 and deformation scale factor of contour is 10.

5.2. Results of the progressive buckling analysis

According to the results in section 5.1, the ratio of inner radius to thickness R_i / t and yield stress σ_y have effect on the failure mode of the cylindrical shell. It is concluded that plastic buckling load is the critical load when the ratio R_i / t is equal to 83.3 and yield stress σ_y is equal to 300MPa. To illustrate the application of the direct approach to progressive buckling design, the cylindrical shell with shell thickness of 12mm, inner radius of 1000mm and yield stress of 300MPa is analyzed. The loading history is shown in Fig. 4.

Based on the approach described in section 4.4, the Bree diagram of cylindrical shell with an opening (a=b=200mm) is shown in Fig. 10. The abscissa is the ratio of axial pressure P to yield stress σ_y and the ordinate is the ratio of thermal loading ΔT to the loading ΔT_i. As shown in Fig. 10, design curves for cycle numbers of 1, 15 and 30 are predicted by the direct approach. It could be found that the axial buckling pressure is decreased with the increasing of thermal loading. In the ratcheting region, with the same thermal loading, the buckling pressure is decreased with the increasing of cycles. It is noted that the thermal loading also has effect on the buckling pressure for the combination of loadings in shakedown region. As shown in Fig. 10, when the thermal loading $\Delta T/\Delta T_i$ is below 1, the progressive buckling design curves for cycle numbers of 1, 15 and 30 are similar because of no ratcheting deformation taking place. In addition, the displacement resulting from thermal loading as well as the thermal stress added to the primary stress result in a little reduction of the progressive buckling pressure. When thermal loading $\Delta T/\Delta T_i$ is greater than 1 in shakedown region, the progressive buckling pressure with the same thermal loading is decreased with increasing of cycle number. This is because the plastic deformation takes place in the first several cycles, and the accumulated plastic deformation is increased with increasing of cycle number. It can be expected that progressive buckling failure may also take place in alternating plasticity region because the ratcheting deformation takes place in the first several cycles.

Besides, the Clement's method is also applied to predict progressive buckling pressure. The key parameters for design point M in Fig. 10 are shown in Table 3, where P_E is the critical Euler pressure, P_L is the limit pressure, P_{b0} is the buckling load in the absence of cyclic secondary stress, P is the progressive buckling pressure, ξ is the stiffness parameter defined in Eq. (4), W is the ratio of secondary stress ΔQ to pressure P and V is the ratio of pressure P to P_{b0}. The results predicted by the design curves in Fig. 5 are shown in Fig. 10. It can be seen that the tendency of the design points predicted by direct approach is the same as that given by Clement's method, but the values of buckling pressure are larger than that predicted by Clement's method. This is because Clement's method would predict conservative result for structure with small cycle number.

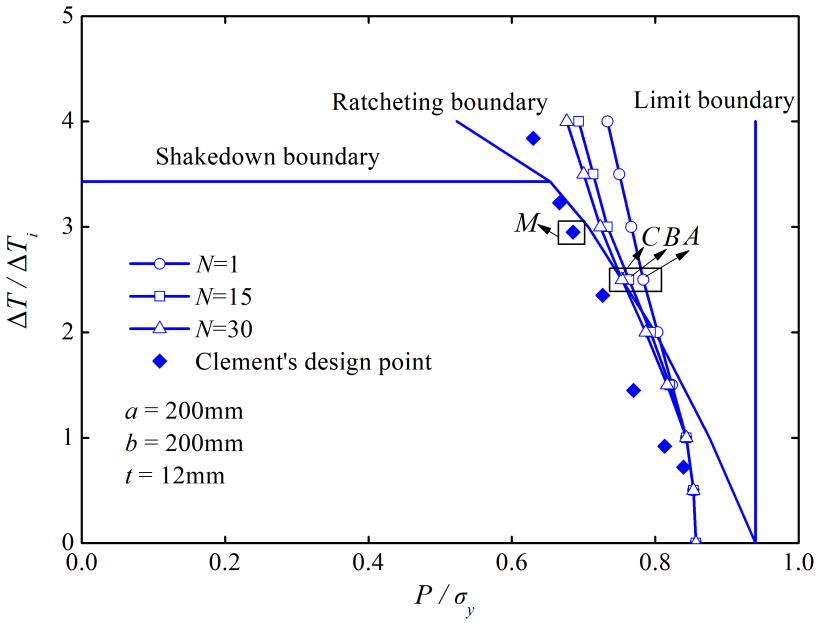

Fig. 10. Bree diagram considering progressive buckling failure of cylindrical shell with semi-major axis a=200mm, semi-minor axis b=200mm and thickness t=12mm. The diamond represents Clement's design point. The solid blue lines with circle, rectangle and triangle represent the cycle number of 1, 15 and 30, respectively. Design points for cycle number of 1, 15 and 30 with $\Delta T/\Delta T_i$=2.5 are shown as point A, B and C, respectively.

Table 3 Parameters for the Clement's method

P_E /MPa	P_L /MPa	P_{b0}/ MPa	P/ MPa	ξ	V	W	ΔT / ΔT_i
469	282	257	206	1.66	0.8	0.64	2.95

Taking the thermal loading $\Delta T/\Delta T_i$=2.5 (points A, B, C in Fig. 10) as an example, the plastic strain distribution of point A at the end of step by step analysis is shown in Fig. 11 and the maximum plastic strain takes place at point D. The maximum plastic strain-cycle number curves at point A, point B and point C in step by step analysis are shown in Fig. 11. The plastic strain at point C is the largest value among the three cases due to the largest cycle number of 30. It can be seen that the increments of plastic strain at point B and point C are decreased with the increasing of cycle. Besides, strain difference between point A and point B ($\Delta\varepsilon_1$ in Fig. 11) is larger than that between point B and point C ($\Delta\varepsilon_2$ in Fig. 11).

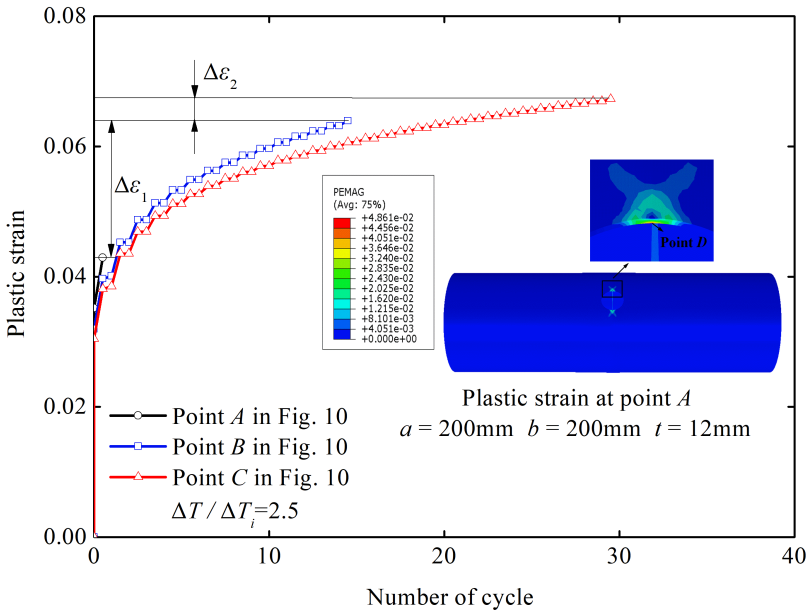

Fig. 11. Plastic strain in step by step analysis with semi-major axis a=200mm, semi-minor axis b=200mm and thickness t=12mm, where the $\Delta T/\Delta T_i$ is equal to 2.5. The maximum plastic strain is shown as point D. The black line with circle, the blue line with rectangle and the red line with triangle represent the relationship between maximum plastic strain and cycle number of design point A, B and C in Fig. 10. $\Delta\varepsilon_1$ is the difference of plastic strain between Point A and Point B and $\Delta\varepsilon_2$ is the difference

between Point B and Point C.

The progressive buckling pressure considering ratcheting deformation is predicted by Riks analysis. The failure mode at point A (see Fig. 10) is shown in Fig. 12. The maximum displacement occurs at point E. The pressure-maximum displacement curves at point A, point B and point C are shown in Fig. 12. The initial displacement of point C resulting from ratcheting deformation is larger than that of point B, and the initial displacement of point A is the least. This is because the ratcheting plastic strain at point C is the largest value among these three cases (see Fig. 11). As mentioned above, the difference of plastic strain $\Delta\varepsilon_1$ is larger than $\Delta\varepsilon_2$, so the displacement difference ΔU_1 is larger than ΔU_2 (see Fig. 12). For the pressure-displacement curve, it is manifested that the pressure increases with the displacement at the start of the analysis. Then, the critical state reaches followed by the unloading process. The maximum pressure in the curve is the buckling pressure. It is seen that the buckling pressure at point A is largest and the smallest pressure is at point C. Besides, the difference of progressive buckling load between point A and point B is larger than that between point B and point C, because the displacement difference ΔU_1 is larger than ΔU_2.

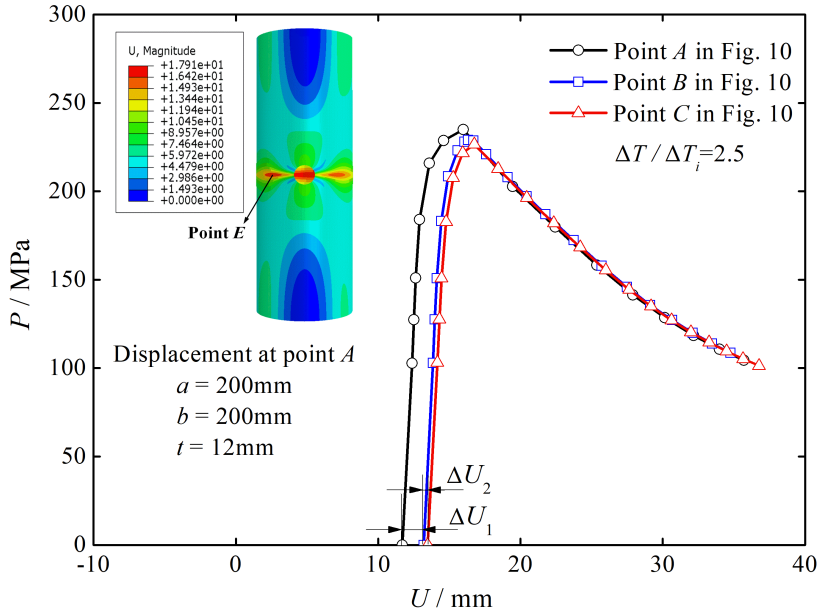

Fig. 12. Pressure-displacement curves in Riks analysis with semi-major axis a=200mm, semi-minor axis b=200mm and thickness t=12mm, where the $\Delta T/\Delta T_i$ is equal to 2.5. The maximum displacement is shown as point E. The black line with circle, the blue line with rectangle and the red line with triangle represent the design point A, B and C

in Fig. 10. ΔU_1 is the difference of initial displacement between Point A and Point B and ΔU_2 is the difference between Point B and Point C.

5.3. Effect of geometrical parameter on progressive buckling pressure

To have a general understanding of the progressive buckling behaviors of the cylindrical shells, their progressive buckling behaviors are investigated with various geometrical parameters. In this section, the effects of opening size as well as the shell thickness are discussed.

5.3.1. Effect of opening size on progressive buckling pressure

The cylindrical shells with semi-major axes of opening a ranging from 200mm to 800mm are investigated. The semi-minor axis of the opening b and thickness t are assumed as 200mm and 12mm, respectively.

The Bree diagram considering progressive buckling predicted by the direct approach is shown in Fig. 13. As the same tendency of limit pressure, the buckling pressure P_{b0} without thermal loading is decreased with the increasing of semi-major axis a. The detailed values of limit pressure P_L and buckling pressure P_{b0} are shown in Table 4. It is found that the limit pressure P_L predicted by the LMM is decreased from 282MPa to 215MPa and buckling pressure predicted by Riks analysis is reduced from 257MPa to 197MPa with semi-major axes of opening a ranging from 200mm to 800mm. The reason for the decreasing of buckling pressure P_{b0} is that the stiffness of the cylindrical shell is decreased with the increasing of semi-major axis of opening a. For the progressive buckling pressure, the shape of design curves in Fig. 13 are similar for all the geometries considered here.

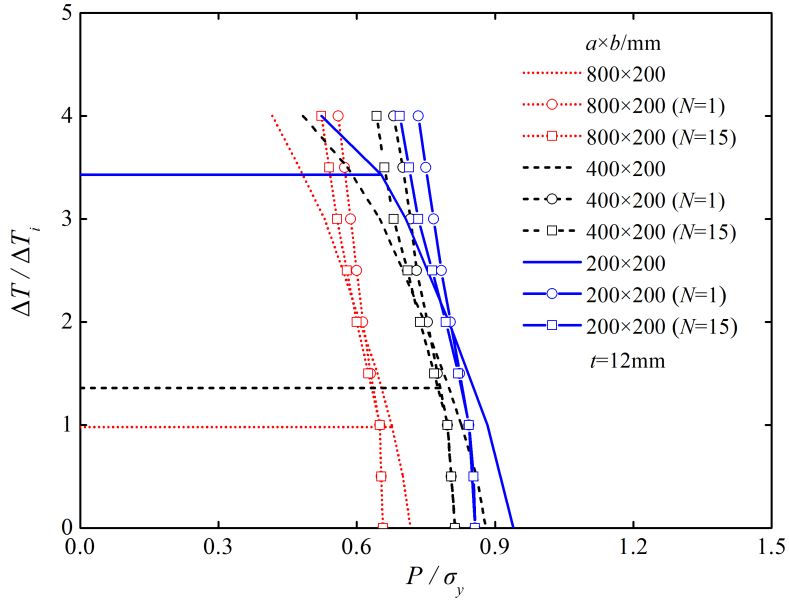

Fig. 13. Progressive buckling curves with various semi-major axes a, where the thickness t is 12mm. The solid blue line, dashed black line and dotted red line show the curves with a×b=200×200, a×b=400×200 and a×b=800×200, respectively. The circle symbol shows the cycle number of 1 and the rectangle represents the cycle number of 15.

Table 4 Limit pressure P_L and buckling pressure P_{b0} for various geometrical parameters

$a\times b$/mm	t/mm	P_L/MPa	P_{b0}/MPa
800×200	12	215	197
400×200	12	264	244
200×200	12	282	257
200×400	12	282	257
200×800	12	282	257
200×200	6	282	198

The cylindrical shells with the semi-minor axes of opening b ranging from 200mm to 800mm are also investigated. The semi-major axis of opening a and thickness t are constant as 200mm and 12mm, respectively.

The progressive buckling curve predicted by the direct approach is shown in Fig. 14. It can be seen that the change of semi-minor axis b has no effect on the buckling pressure P_{b0}, which is the same as limit pressure P_L. This is because the effective cross section area is the same for all cases. The detailed values of limit pressure P_L and buckling pressure P_{b0} are shown in Table 4. It can be seen that the limit pressure P_L is constant as 282MPa and buckling pressure is 257MPa. For the progressive buckling pressure, the design curves in Fig. 14 with various geometries are the same as the cylindrical shell with a=b=200mm mentioned in section 5.2. It is concluded that the cyclic thermal load and the cycle number have the same effect on the progressive buckling pressure with regardless of the different semi-minor axis of opening.

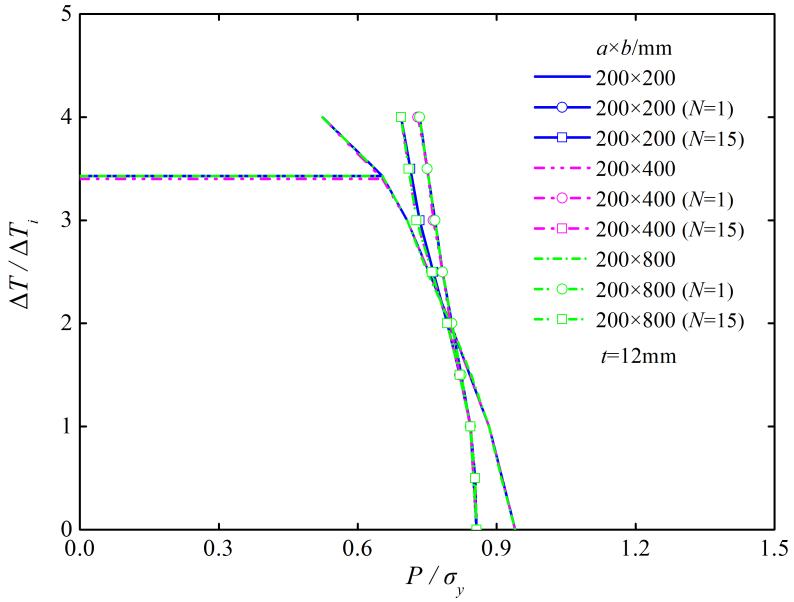

Fig. 14. Progressive buckling curves with various semi-minor axes b, where the thickness t is 12mm. The solid blue line, dashed purple line and dotted green line show the curves with a×b=200×200, a×b=200×400 and a×b=200×800, respectively. The circle shows the cycle number of 1 and the rectangle represents the cycle number of 15.

5.3.2. Effect of cylindrical shell thickness on progressive buckling pressure

The thicknesses t assumed as 6mm and 12mm are considered here to investigate the effect of thickness on progressive buckling behavior. The semi-major axis and the semi-minor axis of the opening are constant as 200mm.

The Bree diagram considering progressive buckling predicted by the direct approach

is shown in Fig. 15. It can be seen that the buckling pressure P_{b0} decreased with the decreasing of thickness t due to the decreasing of stiffness. The detailed results of buckling pressures are shown in Table 4. As shown in Fig. 15, for progressive buckling of cylindrical shell with thickness of 6mm, the less decreased effect of cyclic thermal stress on progressive buckling pressure can be found compared with the thickness of 12mm.

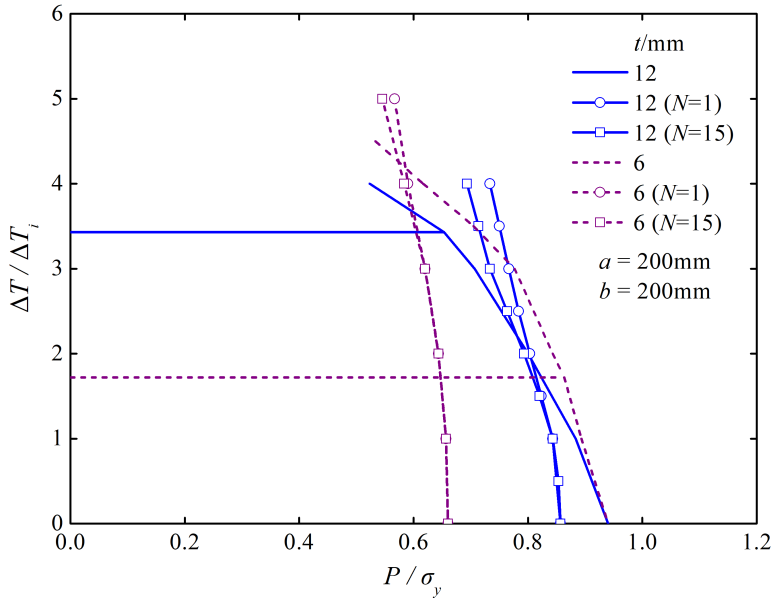

Fig. 15. Progressive buckling curves with various thicknesses t, where a=b=200mm. The solid blue line and dashed purple line show the thickness of 12mm and 6mm. The circle shows the cycle number of 1 and the rectangle represents the cycle number of 15.

5.4. Formula for progressive buckling design

According to the analysis results shown in section 5.3, the semi-major axis of opening a has effect on the progressive buckling pressure, while the effect of semi-minor axis b on the progressive buckling pressure is insignificant. In this part, the yield stress σ_y of abscissa in Figs. 13 and 14 is replaced by limit pressure P_L. Then, the Bree diagram considering progressive buckling failure with various geometrical parameters is shown in Fig. 16. It can be concluded that the progressive buckling design curves are quite similar for models with various parameters.

To apply the direct approach in engineering practice, formulas for progressive buckling design are derive by fitting curves. For thermal loading $\Delta T/\Delta T_i$ <0.5, i.e. the

maximum temperature range of the structure is less than 100℃， the effect of thermal loading on the progressive buckling pressure could be ignored, and the progressive buckling pressure is equal to the buckling pressure in the absence of thermal load P_{b0}. For $\Delta T/\Delta T_i \cong 0.5$, design formula is expressed as Eq. (6), where y denotes the ratio $\Delta T/\Delta T_i$ and x is the ratio P/P_L. The slope K in Eq. (6) is expressed as Eq. (7), which is related to the cycle number N. It can be seen that the increment of slope K is decreased with the increasing of cycle number N. This is because the decreased effect of thermal stress on progressive buckling pressure is reduced with the increasing cycle number N. From the fitting result shown in Fig. 17, it is seen that the formula gives excellent fit, so the Eqs. (6) and (7) could be applied to progressive buckling design if the load conditions, boundary conditions, etc. are the same as those described in section 4. As discussed in section 5.3.2, the shell thickness has effect on the design curves. As shown in Fig. 15, the tendency of curves with other thickness is similar to that with thickness of 12mm. As a result, the design formula could be determined by the same method as thickness of 12mm.

$$y = K\,(\,x - 0.91\,) + 0.5 \tag{6}$$

$$K = 2.47 \ln N - 27.03 \tag{7}$$

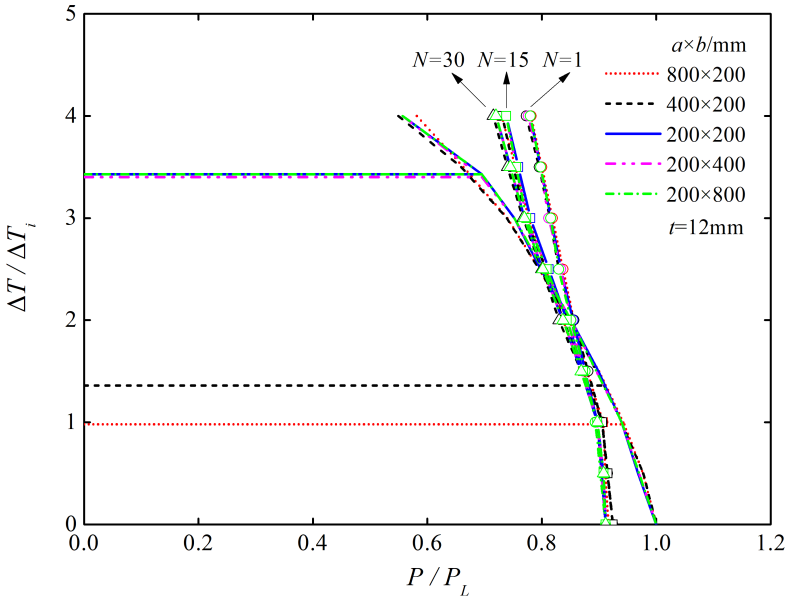

Fig. 16. Bree diagram considering progressive buckling failure with various geometries, where the thickness t is 12mm. The circle, rectangle and triangle represent the cycle number of 1, 15 and 30, respectively.

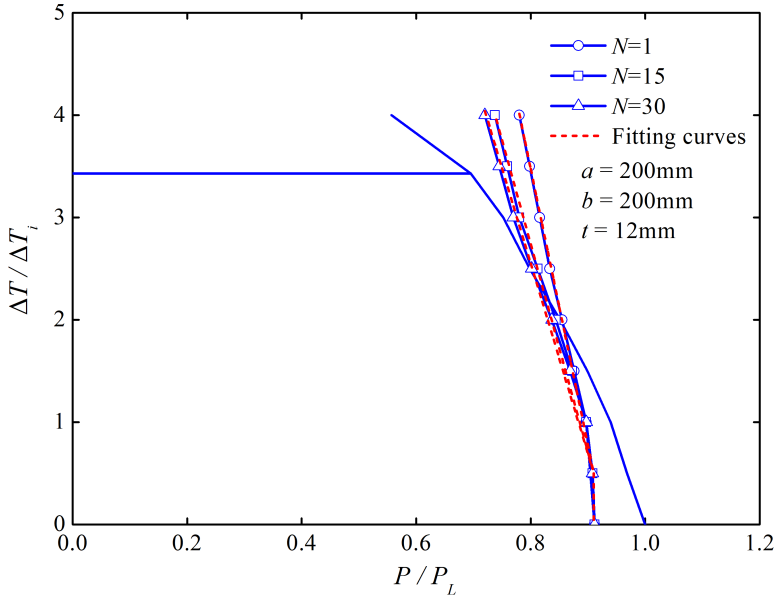

Fig. 17. Fitting curves for progressive buckling design, where the dashed red line is the fitting curves according to Eqs. (6) and (7). The solid blue lines with circle, rectangle and triangle represent the cycle number of 1, 15 and 30, respectively.

It should be stated that there are assumptions made in deriving Eqs. (6) and (7), such as the material follows elastic-perfectly-plastic rule. It can be deduced that if the hardening model is used in analysis, the accumulated strain is smaller than that with elastic-perfectly-plastic model and the progressive buckling pressure with hardening model is larger than that with elastic-perfectly-plastic model. While the progressive buckling pressure with softening model will be smaller than that with elastic-perfectly-plastic model. Besides, material originated plastic strain accumulation could not be modeled by elastic-perfectly-plastic model. For components with both material and structural originated cyclic plastic strain, complex cyclic plasticity rules such as Armstrong and Frederick, Chaboche, Guionnet, Ohno and Wang, etc. have to be used. In progressive buckling analysis, the degradations of material properties with temperature are ignored. The plastic strain accumulation with degraded material properties is larger than that with constant properties, so the progressive buckling pressure with degraded material properties is smaller than that with constant properties.

In addition to the material model, other factors also have effect on the design formulas, such as boundary conditions, opening shape and so on. To get accurate design formulas, the material model, boundary conditions and geometrical parameters should

be determined according to the practical engineering when apply the direct approach in progressive buckling design.

5.5. Further discussions

In present work, the progressive buckling taking place in ratcheting region is considered in the Bree diagram. The research is meaningful for components with lower number of cycle. For example, in nuclear engineering, some components subjected to lower cycles arising from reactor startup and shutdown are no longer within the elastic shakedown range and ratcheting mechanism appears in some local region of these components. If the applied cyclic load point is not far away from the ratcheting limit, the plastic strain increment per cycle may not be very large and the accumulated ratcheting strain could be acceptably small with limited load cycles [64]. For these cases, if compressive stress takes place, the direct approach proposed in this work could be applied to progressive buckling design.

It is expected that the progressive buckling will also take place in shakedown and alternating plasticity regions. For example, structures with much thinner thickness might suffer from progressive buckling failure in shakedown and alternating plasticity regions based on the results in section 5.3.2. In the next work, the mechanism of progressive buckling in shakedown and alternating plasticity regions will be considered and the results will be reported in our further works.

6. Conclusions

In the present study, the Bree diagram is extended to consider the progressive buckling design and a direct approach for structural progressive buckling design considering ratcheting deformation is proposed. The conclusions drawn through this investigation are shown as follows:

(1) The Bree diagram is extended to the progressive buckling design and the progressive buckling failure occurs in the ratcheting domain.

(2) A direct approach is proposed to structural progressive buckling design. In the first stage of the approach, the traditional Bree diagram is determined by the LMM. In the

second stage, the progressive buckling load could be predicted by Riks analysis. The direct approach could predict accurate progressive buckling load compared with other methods.

(3) Compared with Clement's method, the tendency of the design points predicted by the proposed direct approach is the same as that given by Clement's method, but the values of buckling pressure are larger than that predicted by Clement's method due to the conservatism of Clement's method.

(4) The effects of geometrical parameters on the progressive buckling load of cylindrical shell are investigated. It is found that the decreasing of semi-major axis of opening as well as the increasing of shell thickness could enhance the progressive buckling load, while the semi-minor axis of opening has no effect on the progressive buckling load.

(5) Progressive buckling design curves with various parameters are predicted though the direct approach, and the formulas for progressive buckling design are derived by fitting curves.

Acknowledgments

The authors gratefully acknowledge the supports from the China Scholarship Council, National Natural Science Foundation of China (51828501, 51835503), the Higher Education Discipline Innovation Project (111 Project) under the funding code B13020, University of Strathclyde and East China University of Science and Technology during the course of this work.

References

[1] Timoshenko SP, Gere JM. Theory of elastic stability (2nd edition). New York McGraw-Hill 1961.

[2] Teng JG. Buckling of thin shells: recent advances and trends. Appl. Mech. Rev. 1996; 49: 263-274.

[3] Xuan FZ, Gong JG. Fundamental and approaches for damage mode-based design of pressure vessels. Beijing Science Press 2020.

[4] Fatemi SM, Showkati H, Maali M. Experiments on imperfect cylindrical shells under uniform external pressure. Thin-Walled Structures 2013; 65: 14-25.

[5] Zhu Y, Dai Y, Ma Q, et al. Buckling of externally pressurized cylindrical shell: A comparison of theoretical and experimental data. Thin-Walled Structures 2018; 129: 309-316.

[6] Zhang J, Zhang M, Tang W, et al. Buckling of spherical shells subjected to external pressure: A comparison of experimental and theoretical data[J]. Thin-Walled Structures, 2017, 111: 58-64.

[7] Hutchinson JW. Buckling of spherical shells revisited. Proceedings of the Royal Society A: Mathematical, Physical and Engineering Sciences 2016; 472(2195): 20160577.

[8] Błachut J. Buckling of axially compressed cylinders with imperfect length. Computers & structures 2010; 88(5-6): 365-374.

[9] Donnell LH. A new theory for the buckling of thin cylinders under axial compression and bending. Trans. ASME 1934; 56: 795-806.

[10] Von Karman T, Tsien HS. The buckling of thin cylinderical shell under axial compression. Journal of the Aeronatical Sciences 1941; 8: 303-212.

[11] Miller CD. Buckling Criteria for Torispherical Heads under Internal Pressure. Welding Research Council, Bulletin 444, New York 1999.

[12] Miller CD. Buckling Criteria for Torispherical Heads under Internal Pressure. Journal of Pressure Vessel Technology 2001; 123(3): 318-323.

[13] Liu F, Gong JG, Gao FH, et al. A Creep Buckling Design Method of Elliptical Heads Based on the External Pressure Chart. Journal of Pressure Vessel Technology 2019; 141(3): 031203.

[14] Guo SJ, Wang RZ, Chen H, et al. A comparative study on the cyclic plasticity and fatigue failure behavior of different subzones in CrNiMoV steel welded joint. International Journal of Mechanical Sciences 2019; 150: 66-78.

[15] Ma Z, Chen H, Liu Y, et al. A direct approach to the evaluation of structural shakedown limit considering limited kinematic hardening and non-isothermal effect. European Journal of Mechanics-A/Solids 2020; 79: 103877.

[16] Lamarche CP, Tremblay R. Seismically induced cyclic buckling of steel columns including residual-stress and strain-rate effects. Journal of Constructional Steel Research 2011; 67(9): 1401-1410.

[17] Al-Kaseasbeh Q, Mamaghani IHP. Buckling strength and ductility evaluation of

thin-walled steel stiffened square box columns with uniform and graded thickness under cyclic loading. Engineering Structures 2019; 186: 498-507.

[18] Clement G, Acker D, Lebey J. A practical rule for progressive buckling. Nuclear Engineering and Design 1989; 111(2): 209-216.

[19] Zheng XT, Wu KW, Wang W, et al. Low cycle fatigue and ratcheting behavior of 35CrMo structural steel at elevated temperature. Nuclear Engineering and Design 2017; 314: 285-292.

[20] Peng H, Liu Y, Chen H, et al. Shakedown analysis of engineering structures under multiple variable mechanical and thermal loads using the stress compensation method. International Journal of Mechanical Sciences 2018; 140: 361-375.

[21] Varvani-Farahani A, Nayebi A. Ratcheting in pressurized pipes and equipment: A review on affecting parameters, modelling, safety codes, and challenges. Fatigue & Fracture of Engineering Materials & Structures 2018; 41(3): 503-538.

[22] Zheng X, Peng H, Yu J, et al. Analytical ratchet limit for pressurized pipeline under cyclic nonproportional loadings. Journal of Pipeline Systems Engineering and Practice 2017; 8(3): 04017002.

[23] Pei X, Dong P. A universal approach to ratcheting problems of Bree type incorporating arbitrary loading and material nonlinearity conditions. International Journal of Pressure Vessels and Piping 2020; 185: 104137.

[24] Beesley R, Chen H, Hughes M. A novel simulation for the design of a low cycle fatigue experimental testing programme. Computers & Structures 2017; 178: 105-118.

[25] Bree J. Elastic-plastic behaviour of thin tubes subjected to internal pressure and intermittent high-heat fluxes with application to fast-nuclear-reactor fuel elements. J. Strain Anal. Eng. Des. 1967; 2 (3): 226–238.

[26] Bree J. Plastic deformation of a closed tube due to interaction of pressure stresses and cyclic thermal stresses. International journal of mechanical sciences 1989; 31(11-12): 865-892.

[27] Seshadri R. Inelastic evaluation of mechanical and structural components using the generalized local stress strain method of analysis. Nuclear Engineering and Design 1995; 153 (2–3): 287–303.

[28] Simon JW. Direct evaluation of the limit states of engineering structures exhibiting limited, nonlinear kinematical hardening. Int. J. Plast. 2013; 42: 141–167.

[29] Mackenzie D, Boyle J, Hamilton R. The elastic compensation method for limit and

shakedown analysis: a review. J. Strain Anal. Eng. Des. 2000; 35 (3): 171–188.

[30] Chen H, Ponter AR. Shakedown and limit analyses for 3-D structures using the linear matching method. Int. J. Press. Vessel. Pip. 2001; 78 (6): 443–451.

[31] Chen H, Ponter AR. A method for the evaluation of a ratchet limit and the amplitude of plastic strain for bodies subjected to cyclic loading. European Journal of Mechanics-A/Solids 2001; 20(4): 555-571.

[32] Ponter AR, Chen H. A minimum theorem for cyclic load in excess of shakedown, with application to the evaluation of a ratchet limit. European Journal of Mechanics-A/Solids 2001; 20(4): 539-553.

[33] Chen H. Lower and upper bound shakedown analysis of structures with temperature-dependent yield stress. J. Press. Vessel Technol. 2010; 132 (1): 011202.

[34] Chen H, Ponter AR. A direct method on the evaluation of ratchet limit. J. Press. Vessel Technol. 2010; 132 (4): 041202.

[35] Brouard D, Cousseran P, Lebey J, et al. Progressive buckling by cyclic straining. Proceedings SMiRT 6 Paris 1981.

[36] Quoc SN, Gary G, Baylac G. Interaction buckling-progressive deformation. Nuclear Engineering and Design, 1983; 75(2): 235-243.

[37] Devos J, Gontier G, Hoffmann A. Buckling Induced by Cyclic Straning: Analysis of Simple Models. 7th SMiRT Chicago 1983.

[38] Wagner HNR, Hühne C, Khakimova R. On the development of shell buckling knockdown factors for imperfection sensitive conical shells under pure bending. Thin-Walled Structures 2019; 145: 106373.

[39] Lee A, López Jiménez F, Marthelot J, et al. The geometric role of precisely engineered imperfections on the critical buckling load of spherical elastic shells. Journal of Applied Mechanics 2016; 83(11): 111005.

[40] Evkin A, Kolesnikov M, Lykhachova O. Buckling load prediction of an externally pressurized thin spherical shell with localized imperfections. Mathematics and Mechanics of Solids 2019; 24(3): 653-667.

[41] Li K, Zheng J, Liu S, et al. Buckling behavior of large-scale thin-walled ellipsoidal head under internal pressure. Thin-Walled Structures 2019; 141: 260-274.

[42] Ahn K, Lim IG, Yoon J, et al. A simplified prediction method for the local buckling load of cylindrical tubes. International Journal of Precision Engineering and Manufacturing 2016; 17(9): 1149-1156.

[43] Gong JG, Yu L, Wang F, et al. Effect of welding residual stress on the buckling behavior of storage tanks subjected to harmonic settlement. Journal of Pressure Vessel Technology 2017; 139(1): 011401.

[44] Zhu Y, Dai Y, Ma Q, et al. Buckling of externally pressurized cylindrical shell: A comparison of theoretical and experimental data. Thin-Walled Structures 2018; 129: 309-316.

[45] Szymczak C, Kujawa M. Flexural buckling and post-buckling of columns made of aluminium alloy. European Journal of Mechanics-A/Solids 2019; 73: 420-429.

[46] Li K, Zheng J, Zhang Z, et al. Experimental investigation on buckling of ellipsoidal head of steel nuclear containment. Journal of Pressure Vessel Technology 2017; 139(6): 061206.

[47] Jimbo M, Hirayama H, Matsuura S. Buckling Analysis of Cylinder with Free Fdge under Thermal Load. SMiRT 15 Seoul Korea 1999.

[48] Koo GH, Lee JH. Progressive buckling analysis for a cylindrical shell structure with the free edge subjected to moving thermal cycles. International journal of pressure vessels and piping 2004; 81(5): 409-418.

[49] Dicleli M, Mehta A. Simulation of inelastic cyclic buckling behavior of steel box sections. Computers & structures 2007; 85(7-8): 446-457.

[50] Hassan MS, Salawdeh S, Goggins J. Determination of geometrical imperfection models in finite element analysis of structural steel hollow sections under cyclic axial loading. Journal of Constructional Steel Research 2018; 141: 189-203.

[51] Shariati M, Hatami H, Torabi H, et al. Experimental and numerical investigations on the ratcheting characteristics of cylindrical shell under cyclic axial loading. Structural Engineering and Mechanics 2012; 44(6): 753-762.

[52] ABAQUS. Abaqus documentation (v.6.14). Simulia Dassault Systémes 2014.

[53] French Society for Design and Construction Rules for Nuclear Island Components. Afcen RCC-MRx code: Design and construction rules for nuclear power cenerating stations. Paris 2015.

[54] Murakami T, Yoguchi H, Hirayama H, et al. The effect of thermal ratchetting deformation on buckling strength of cylindrical shells in bending. SMiRT 13 Brazil 1995.

[55] Mahbadi H, Eslami MR. Cyclic loading of beams based on the Prager and Frederick–Armstrong kinematic hardening models. International journal of mechanical sciences 2002; 44(5): 859-879.

[56] Jiang W. Shakedown analysis of hollow spheres. Journal of engineering mechanics 1994; 120(7): 1447-1480.

[57] Abdalla HF, Younan MYA, Megahed MM. Shakedown limit load determination for a kinematically hardening 90 deg pipe bend subjected to steady internal pressures and cyclic bending moments. Journal of pressure vessel technology 2011; 133(5): 051212.

[58] Abdalla HF. Shakedown Limit Load Determination of a Cylindrical Vessel–Nozzle Intersection Subjected to Steady Internal Pressures and Cyclic in-Plane Bending Moments. Journal of Pressure Vessel Technology 2014; 136(5): 051602.

[59] ASME. Boiler and pressure vessel code section III subsection NH, rules for construction of nuclear facility components: Class 1 components in elevated temperature service. New York American Society of Mechanical Engineers 2015.

[60] Cinoglu IS, Begley MR, Deaton JD, et al. Elastoplastic design of beam structures subjected to cyclic thermomechanical loads. Thin-Walled Structures 2019; 136: 175-185.

[61] Nefussi G, Combescure A. Coupled buckling and plastic instability for tube hydroforming. International Journal of Mechanical Sciences 2002; 44(5): 899-914.

[62] Han H, Cheng J, Taheri F, et al. Numerical and experimental investigations of the response of aluminum cylinders with a cutout subject to axial compression. Thin-Walled Structures 2006; 44(2): 254-270.

[63] Shariati M, Rokhi MM. Numerical and experimental investigations on buckling of steel cylindrical shells with elliptical cutout subject to axial compression. Thin-Walled Structures 2008; 46(11): 1251-1261.

[64] Chen HF, Ponter AR. Integrity assessment of a 3D tubeplate using the linear matching method. Part 1. Shakedown, reverse plasticity and ratchetting. International journal of pressure vessels and piping 2005; 82(2): 85-94.